Silicon-Integrated Lead-Free $BaTiO_3$-Based Film Capacitors with Excellent Energy Storage Performance and Highly Stable Irradiation Resistance

Fan Zhao,[ab] Yilin Wu,[ab] Yanzhu Dai,[ab] Guangliang Hu,[ab] Ming Liu,*[ab] Runlong Gao,[cd] Linyue Liu,*[c] Xin Liu,[e] Yonghong Cheng,*[e] Tianyi Hu,[b] Chunrui Ma,[b] Dengwei Hu,[f] Xiaoping Ouyang[c] and Chun-Lin Jia[abg]

[a] *School of Microelectronics, Xi'an Jiaotong University, Xi'an 710049, China*

[b] *State Key Laboratory for Mechanical Behavior of Materials, Xi'an Jiaotong University, Xi'an 710049, China*

[c] *State Key Laboratory of Intense Pulsed Radiation Simulation and Effect, Northwest Institute of Nuclear Technology, Xi'an 710024, China*

[d] *School of Nuclear Science and Technology, Xi'an Jiaotong University, Xi'an 710049, China*

[e] *State Key Laboratory of Electrical Insulation and Power Equipment, School of Electrical Engineering, Xi'an Jiaotong University, Xi'an 710049, China*

[f] *Faculty of Chemistry and Chemical Engineering, Engineering Research Center of Advanced Ferroelectric Functional Materials, Key Laboratory of Phytochemistry of Shaanxi Province, Baoji University of Arts and Sciences, 1 Hi-Tech Avenue, Baoji, Shaanxi, 721013 P. R. China*

[g] *Ernst Ruska Centre for Microscopy and Spectroscopy with Electrons, Forschungszentrum Jülich, D-52425 Jülich, Germany*

* Email address: m.liu@xjtu.edu.cn; 13619269436@163.com； cyh@xjtu.edu.cn

Abstract:

Silicon integrated lead-free oxide thin film capacitors with high energy storage density (W_{re}), high efficiency (η) and good thermal stability have great application potential in modern communication field. Here, 1 mol% SiO_2-doped $Ba(Zr_{0.35}Ti_{0.65})O_3$ (BZTS) thin film capacitors are integrated on the Si and HfO_2 buffered Si substrates by radio-frequency magnetron sputtering system. It is found that the energy storage performances are significantly improved by inserting an HfO_2 buffer layer (about 13.5 nm) between the BZTS layer and the Si substrate. The improved W_{re} of the BZTS/HfO_2 thin film capacitors can be up to 93.48 J/cm^3 at room temperature, which is by about 65% higher than that of the film without the HfO_2 buffer layer, and the η~71.44%. Moreover, the introduction of the HfO_2 buffer layer leads to a superior thermal stability in the wide temperature range from -100 °C to 200 °C with a very small change rate of ~3.39%. Under different irradiations with doses of the He^+ from 1×10^{12} ions/cm^2 to 7×10^{15} ions/cm^2 and neutrons from 5×10^{12} ions/cm^2 to 1×10^{14} ions/cm^2, the BZTS thin film capacitors with HfO_2 buffer layer show ultra-stable energy storage performance. Our research provides an effective strategy for the integration of high performance BZTS thin film capacitors on Si substrates, and our results demonstrate potential of the Si integrated thin film capacitors for the application in nuclear technology, space station, satellite, radiation center and other harsh environments.

Keywords: Thin film capacitors, Energy storage density, Thermal stability， High temperature, Irradiation resistance.

1. Introduction

With the continuous consumption of global energy and the increasingly serious problem of environmental pollution, the demand for renewable energy is increasing day by day. How to solve the problem in energy storage has become a hot topic of current research. Compared with electrochemical capacitors, supercapacitors and batteries, dielectric capacitors have faster discharge speed, higher power density and longer service life, which have become the focus of academic and industrial research in recent years.[1-4] Normally, the energy storage density (W_{re}), the energy loss density (W_{loss}) and the efficiency (η) of dielectric materials are defined as:

$$W_{re} = \int_{P_r}^{P_{max}} EdP \quad (1)$$

$$W_{loss} = \int PdE \quad (2)$$

$$\eta = \frac{W_{re}}{W_{re}+W_{loss}} \quad (3)$$

where P_{max} and P_r are the maximum polarization and remnant polarization of the material, respectively. E is the applied electric field. In order to design a dielectric energy storage device with good useable performance, the selected dielectric materials need to simultaneously meet the requirements of large P_{max}, small P_r and high electric breakdown strength (E_b).[5] Dielectric materials for energy storage can usually be divided into four types: linear dielectric, ferroelectric, relaxed ferroelectric and antiferroelectric.[6-9] Among these types, relaxor ferroelectric dielectric is one of the ideal candidate materials for energy storage capacitors due to its slim hysteresis loop with high P_s and low P_r. Most of the relaxor ferroelectric thin films with better energy storage properties have been reported to be lead-based (Pb-based) materials. Such as $0.68Pb(Mg_{1/3}Nb_{2/3})O_3$-$0.32PbTiO_3$,[10] $Pb_{0.9}La_{0.1}(Zr_{0.52}Ti_{0.48})O_3$,[11] and $Pb(Zr_{0.53}Ti_{0.47})_{0.90}Sc_{0.10}O_3$.[12] It is well known that Pb-based materials is harmful for human health and the environment, and thus their applications will be seriously limited in the future. Therefore, it is an urgent task to seek a high-performance lead-free relaxation ferroelectric material to meet the practical application.

Recently, a lead-free relaxor ferroelectric $Ba(Zr_xTi_{1-x})O_3$ thin film has attracted much attention due to its high dielectric constant, good thermal stability and relatively high energy storage performance.[13-15] $Ba(Zr_xTi_{1-x})O_3$ thin films have been prepared by different methods (sol-gel, magnetron sputtering, etc.) on various substrates ($LaAlO_3$, $SrTiO_3$, MgO, etc.).[16,17] However, the energy storage performance of $Ba(Zr_xTi_{1-x})O_3$ thin films grown on Si substrates have not been reported. Si is the basic material of current and even future integrated circuits and MEMS devices.[18-22] Therefore, to integrate the energy storage devices on Si substrates is an important step in facilitating the industrial application and rapid promotion of energy storage devices.

In this paper we propose a new strategy to improve the energy storage performance of $Ba(Zr_{0.35}Ti_{0.65})O_3$ (BZT) thin film capacitors by adding a buffer layer on the Si substrate. According to our previous studies,[23] According to our previous studies,[23] the E_b of BZT films can be improved by a small amount of doping SiO_2 with low dielectric constant and excellent electrical insulation property in BZT target. In this work, the 1 mol% SiO_2 doped BZT (BZTS) thin films are fabricated on Si and HfO_2 buffered Si substrates by radio-frequency (RF) magnetron sputtering system, respectively. The effects of the HfO_2 buffer layer on the BZTS thin film's structure, ferroelectric performance, energy storage performance and thermal stability are mainly studied. The results show that the enhancement of P_{max} and E_b is achieved by inserting the buffer layer. An ultra-high W_{re}~93.48 J/cm^3 for the BZTS/HfO_2 thin film at room temperature (RT) was obtained, which is about 65% higher than the W_{re}~56.66 J/cm^3 of the BZTS thin film without the HfO_2 buffer layer. Besides, the η of BZTS thin film capacitors with and without HfO_2 buffer layer are 71.44% and 70.99%, respectively. In addition, the HfO_2 buffer layer can also significantly improve the thermal stability of the BZTS thin film capacitors. At the same time, in order to expand the application of Si integrated BZTS thin film capacitors in harsh environment, we also investigate the influence of different doses of He^+ and neutron irradiation on the energy storage performance of the Si integrated BZTS thin film

capacitors.

2. Experimental

Before the BZTS thin film growth, the native SiO_2 layer on p-type Si (100) substrates was etched by a hydrofluoric acid etch. The HfO_2 buffer layer with a thickness of about 13.5 nm was deposited on the p-type Si (100) substrate at 280 °C using plasma enhanced atomic layer deposition (ALD) technique, and the thickness was determined from Fig. S1. Then, the optimized BZTS thin films with thickness ~415 nm was deposited on both Si and HfO_2/Si substrates by a RF magnetron sputtering system, respectively. The energy storage performances of BZTS thin films on HfO_2/Si substrates as function of thickness of BZTS are shown in Fig. S2 and S3. All thin films were grown under 700 °C and 0.2 mbar of Ar/O_2 (1:1) mixing pressure. After the growth, all the BZTS thin films were *in situ* annealed at 700 °C for 15 min under the Ar/O_2 mixture pressure of 200 mbar, and then naturally cooled down to RT.

The crystal structures of the BZTS thin films were characterized by the high-resolution X-ray diffraction (HRXRD) of PANalytical X'Pert MRD. The microstructure and phase composition of the thin films were investigated by scanning transmission electron microscopy (STEM) and the energy dispersive X-ray energy dispersion spectroscopy (EDS) mapping was performed on a JEOL ARM 200F electron microscope. For measurements of the dielectric/ferroelectric properties of the BZTS film, 100 nm thick Pt top electrodes with size of 200 μm × 200 μm were deposited on the BZTS film using RF sputtering with a shadow mask. The top-to-bottom electrode configuration was used to apply the electric field. The dielectric constant (ε_r) and dielectric loss ($\tan\delta$) were characterized depending on both frequency (100 Hz~1 MHz) at RT and temperature (0~500 °C) at 1 kHz by Keysight E4980AL Precision LCR Meter. The first order reversal curve (FORC) loops and ferroelectric (*P*-*E*) hysteresis loops were characterized using TF Analyzer 2000 E with the input wave of a triangular wave at 40 Hz and 1 kHz respectively. The *P*-*E* loops of different temperature were controlled through Lakeshore cryo-cooled probe station

(CRX-6.5K, Lake Shore Cryotronics, Inc., USA). The leakage current density curve of the BZTS thin films was measured with a step scan duration of 2 seconds by TF Analyzer 2000 E at RT.

The He^+ irradiation was performed in a 4 MV electrostatic accelerator located at Shanghai Institute of Applied Physics (Chinese Academy of Science) with an energy of 3 MeV, and the irradiation doses were 1×10^{12}, 1×10^{13}, 5×10^{14}, 1×10^{15} and 7×10^{15} ions/cm^2, respectively. The neutron irradiation was performed at Xi'an Pulsed Reactor located at Northwest Institute of Nuclear Technology with an average energy of 1 MeV, and the irradiation dose was 5×10^{12}, 3×10^{13}, 7×10^{13} and 1×10^{14} ions/cm^2, respectively.

3. Results and discussion

The XRD θ-2θ scanning of the BZTS films are shown in Fig. 1a. It can be seen that the BZTS thin films on the Si substrates with and without HfO_2 buffer layer are all perovskite-phase polycrystalline films without any secondary phases. However, the BZTS thin film grown on the HfO_2 buffered substrate has a relatively stronger diffraction peak intensity than the BZTS thin film grown directly on the Si (100) substrate. The enhancement of the diffraction peak may be due to the increase of the grain size in the BZTS film caused by the HfO_2 buffer layer.[24] Fig. 1b and Fig.1c shows low-magnification dark field STEM images of the BZTS thin films without and with HfO_2 buffer layer, respectively. The corresponding selected area electron diffraction (SAED) patterns are shown in the insets of Fig. 1b and Fig.1c were recorded in the region of the BZTS thin films. The results show that the SAED patterns of the BZTS thin films grown on Si substrates show obvious polycrystalline diffraction rings with or without HfO_2 buffer layer. EDS was used to map the distribution of chemical elements in the region within the red box in Fig. 1c, and the details are shown in Fig. 1d. The spatial distribution of Ba, Ti, Hf and O elements in different layers can be seen clearly, which further confirms the HfO_2 buffer layer.

It is obvious from formula (1) that the E_b of the capacitors is an important

parameter for improving the recoverable energy. The E_b of both the BZTS thin film capacitors with and without HfO_2 buffer layer were analyzed by the Weibull distribution function,[25] and the details are shown in Fig. 2a. It is noted that the addition of the HfO_2 layer leads to an enhancement of E_b from ~6.92 MV/cm to ~8.78 MV/cm. It is well known that the leakage current density (J) directly affect the E_b of ferroelectric film capacitor. The leakage current density varying with the electric field (J-E) of the BZTS and BZTS/HfO_2 thin film capacitors at RT are shown in Fig. 2b. The leakage current density at the electric field of ±1 MV/cm is below 5×10^{-7} A/cm^2 for both the BZTS and BZTS/HfO_2 thin film capacitors, which is much lower than the reported values of the BZT thin film capacitors.[26] This phenomenon is mainly attributed to the doping of SiO_2 in BZT target. The SiO_2 always show high electrical insulation, which can be improve the insulation characteristics of the BZT thin film capacitors. Meanwhile, the leakage current density of the BZTS thin film capacitors with HfO_2 buffer layer is lower than that of the film without HfO_2 buffer layer in the whole test electric field range at the same thickness (~ 430 nm), which is mainly due to the good insulation of the HfO_2 buffer layer that hinders the free electron movement in the BZTS thin films. In order to understand the contribution of the HfO_2 buffer layer to the improvement of the E_b of thin film capacitors. A numerical simulation based on the finite element method was performed for the research samples. Fig. 2c and Fig. 2d are the electric tree path diagrams in the BZTS and the BZTS/HfO_2 thin film capacitors, respectively, under different applied electric fields of 2.3 MV/cm, 4.7 MV/cm and 7.2 MV/cm. It can be clearly seen that the spread of electric tree branches in both film capacitors increase as the increase of external electric field. When the electric field reaches 7.2 MV/cm, the electric branch penetrates whole thickness of the BZTS thin film capacitors without HfO_2 buffer layer from the top electrode to the bottom electrode, breaking down the device. In comparison, in the BZTS thin film capacitors with HfO_2 buffer layer the electric branch stops at position before the BZTS/HfO_2 interface under the electric field of 7.2

MV/cm. This means that the BZTS thin film capacitors with HfO_2 buffer layer have higher E_b than that without HfO_2 buffer layer. The addition of the buffer layer reduces the potential in BZTS layer to a too small value to accelerate the free electrons to a sufficiently high energy state, and thus greatly restricts the growth of electrical branches, resulting in significantly improved breakdown field strength of the film. In addition, we note that the results of the E_b obtained by experiment and simulation are slightly different, which can be interpreted as the influence of unavoidable defects in actual materials.

Besides the E_b, the difference between P_{max} and P_r is another parameter to determine the energy storage performance. The value of P_{max} and P_r in nature is controlled by the mechanism of domain switching. The first order reversal curve (FORC) is an effective method to characterize polarization characteristics. Here, we set E_{max} = 3.6 MV/cm, $\Delta E_r = \Delta E$ = 0.12 MV/cm and totally 60 FORC loops were measured. The selected loops are shown in Fig. 3a and Fig. 3b. The FORC distribution density can calculated by the formula $\rho(E_r, E) = \frac{1}{2}\frac{\partial P^2(E_r,E)}{\partial E_r \partial E}$ according to the FORC loops, where $P(E_r, E)$, E and E_r corresponding to the polarization of the FORC loop, the real electric field and the reversal electric field, respectively. The FORC distribution of the BZTS thin films without HfO_2 buffer layer (Fig. 3c) exhibits a low-density distribution zone around the central region, which can be understood as ferroelectric domain switching in the low electric field and can contribute to the relative larger P_{max} in Fig. 3a. Compared to Fig. 3c, the FORC distribution of the BZTS thin films with HfO_2 buffer layer (Fig. 3d) is more uniform, indicating a lower coercive electric field corresponding to a weak ferroelectric polarization behavior and more stable relaxor ferroelectric state. This can contribute to a slimmer *P-E* loop and reduce the hysteresis loss.

Fig. 4a shows the frequency dependence of ε_r and tanδ of the BZTS and the BZTS/HfO_2 thin films at RT. It can be seen that ε_r of both BZTS and BZTS/HfO_2 thin films decreases with the increase of frequency. The ε_r of the BZTS/HfO_2 thin films is

lower than that of BZTS thin films, which is mainly due to the low ε_r of the HfO_2 buffer layer and the BZTS/HfO_2 structure that is equivalent to the series connection of the ferroelectric and the dielectric layer.[27,28] In fact, the moderate ε_r of the BZTS thin films with HfO_2 buffer layer actually assists to obtain the high energy density with the enhanced E_b. The tanδ of the BZTS and BZTS/HfO_2 thin films shows no significant differences in the frequency range of 100 Hz ~ 1 MHz. Fig. 4b shows the *P-E* hysteresis loops of the BZTS and BZTS/HfO_2 thin film capacitors. The P_{max} of the BZTS/HfO_2 thin films with high E_b can reach 34.47 μC/cm^2, which is higher than of the BZTS thin films (28.17 μC/cm^2). Based on the results of E_b and polarization of the BZTS and BZTS/HfO_2 thin film capacitors, the energy storage performance changes were investigated at RT. The W_{re} and η of the BZTS and BZTS/HfO_2 thin film capacitors obtained from the corresponding *P-E* loops as function of electric field are presented in Fig. 4c. It is clearly seen that the W_{re} increases with the increases of applied electric field and reaches the maximum value of 56.66 J/cm^3 for the capacitor without buffer layer at 6.07 MV/cm and 93.48 J/cm^3 for the film with buffer layer at 8.53 MV/cm. The W_{re} of the BZTS thin film capacitors with the HfO_2 buffer is by ~ 65% higher than that of the film without HfO_2 buffer. In addition, the η of BZTS thin film capacitors with and without HfO_2 buffer layer are 71.44% and 70.99%, respectively. All these results demonstrate that the energy storage performance of silicon integrated BZTS thin film capacitors is significantly improved through inserting HfO_2 buffer layer. In addition, it is well known that excellent ferroelectric fatigue durability is a necessary condition for dielectric capacitors to achieve long-term stable charging and discharging. Fig. 4d shows the fatigue properties of W_{re} and η for the BZTS/HfO_2 thin film capacitors under 7.7 MV/cm at RT. The energy storage performance of the BZTS/HfO_2 thin film capacitors has no obvious degradation after continuous cycling (1×10^6 cycles). The variation of W_{re} and η of the BZTS/HfO_2 thin film capacitors are only 0.56% and 1.07%, respectively, which shows that BZTS/HfO_2 thin film capacitors have excellent fatigue properties at RT.

As we know, thermal stability is a key factor to determine the application of materials in electronic devices. Fig. 5a shows the temperature dependence of ε_r and tanδ at 1 kHz for the BZTS thin film capacitors and the BZTS/HfO_2 thin film capacitors. It can be clearly seen that the ε_r and tanδ of the BZTS film capacitors with HfO_2 buffer layer are almost unchanged within the test temperature range, indicating that the thermal stability of the film capacitors is significantly improved after the insertion of the HfO_2 buffer layer. This may be attributed to the high thermal stability of the HfO_2 layer and the high interface quality on silicon.[29] In order to further explore the effect of HfO_2 buffer layer on improvement of the thermal stability of the film capacitors, the energy storage performances for the BZTS thin film capacitors and the BZTS/HfO_2 thin film capacitors were investigated by measuring the *P-E* loops in the temperature range from -100 °C to 200 °C, and the obtained W_{re} and η are summarized in Fig. 5b. The W_{re} of BZTS thin film capacitors with HfO_2 buffer layer can reach ~ 48.08 J/cm^3 at 200 ℃ and its change rate is only ~3.39%, which is much lower than that of the film without HfO_2 buffer layer (~22.47%). At the same time, the η of the film with the HfO_2 buffer layer are still higher than 65.05% even at high temperature, which is much superior to 36.33% for the film without HfO_2 buffer layer. All of these results indicate that the introduction of an HfO_2 buffer layer can significantly improve the thermal stability of BZTS thin film capacitors for integration on Si substrate. In order to further verify the thermal stability of the BZTS/HfO_2 thin film capacitors, the fatigue behavior of the BZTS/HfO_2 thin film capacitors were measured under 5.35 MV/cm at 200 °C (as shown in Fig. 5c). The results show that the W_{re} and η of the BZTS/HfO_2 thin film capacitors have no obvious signs of attenuation during the entire charge-discharge process. The changes of W_{re} and η in 10^6 cycles are both less than 5%, showing the excellent fatigue performance of the dielectric capacitor at high temperatures. From Fig. 5d, it can be seen that both the energy storage density and the working temperature of the BZTS thin film capacitors with HfO_2 buffer layer are superior to the reported lead-free and

lead-based films prepared by physical methods on Si substrates.

In order to further explore the energy storage performance in harsh environment, we also studied the influence of He^+ and neutron irradiation at different doses on the energy storage performance of Si integrated BZTS thin film capacitors. Fig. 6a shows *P-E* hysteretic loops at RT of the BZTS/HfO_2 thin film capacitors after different doses of He^+ irradiation. The irradiation energy is 3 MeV and applied electric field is 8.2 MV/cm. It is noted that with the increase of irradiation dose, the *P-E* hysteresis loops of the BZTS/HfO_2 thin film capacitors do not change significantly compared with the unirradiated sample. The E_b of the BZTS/HfO_2 thin film capacitors irradiated by He^+ ions with different doses were analyzed using the Weibull distribution function (as shown in Fig. S4), and the W_{re} and η were obtained by calculating the *P-E* hysteresis loops of the thin film capacitors after He^+ irradiation. Fig. 6b summarizes the changes of W_{re}, η and E_b after He^+ irradiation, and the dotted line represents the energy storage performance of the unirradiated samples. It can be seen that, the W_{re}, η and E_b of the BZTS/HfO_2 thin film capacitors do not significantly change with the increase of He^+ irradiation dose, and the variation of W_{re}, η and E_b are only about 7.73%, 2.76% and 2.87%, respectively. Fig. 6c shows the *P-E* hysteretic loops of the BZTS/HfO_2 thin film capacitors at RT after neutron irradiation with different doses (irradiation energy of 1 MeV and applied electric field of 8.2 MV/cm). From Fig. 6c, it can be seen that the P_{max} increases slightly with the increase of neutron irradiation dose, while the P_r shows stable. The W_{re}, η and E_b (from Fig. S5) of the BZTS/HfO_2 thin film capacitors after neutron irradiation with different doses are summarized in Fig. 6d, and the dotted line represents the energy storage performance of the unirradiated samples. The results show that with the increase of neutron irradiation dose, the variation of W_{re}, η and E_b of the BZTS/HfO_2 thin film capacitors are only 4.62%, 3.69% and 5.29%, respectively. In general, He^+ irradiation would mainly introduce displacement damage inside the materials, while neutron irradiation would introduce a large number of vacancy defects. Compared with He^+ irradiated samples, the E_b of the BZTS/HfO_2

thin film capacitors after neutron irradiation decreases more greatly, which may be attributed to the fact that vacancy defects introduced in dielectric materials are more likely to cause the degradation of E_b of dielectric film capacitors than displacement damage. Although the energy storage performance of the samples after He^+ irradiation and neutron irradiation vary to some extent, the overall rate of change is still much lower than the requirement of industry (±15%), and thus we can still consider that the BZTS/HfO_2 thin film capacitors has a good irradiation resistance.

4. Conclusions

In conclusion, both the energy storage density and thermal stability are largely improved by inserting a high resistance dielectric HfO_2 buffer layer between the BZTS thin film and the Si substrate. The W_{re} of the BZTS thin film capacitors with HfO_2 buffer layer can reach to 93.48 J/cm^3 at RT, which is by about 65% higher than that of the film without HfO_2 buffer layer, and the η~71.44%. Besides the enhancement of the energy storage density at RT, the insertion of the HfO_2 buffer layer also results in a superior thermal stability in the wide temperature range from -100 °C to 200 °C with a very low change rate (~3.39%), which is much lower than the requirement of industry (±15%). The enhanced energy storage performances demonstrate that the dielectric buffer layer between relaxor ferroelectric and Si substrate is a feasible way to improve energy storage density and thermal stability of the devices for energy storage application and speed the industrial applications due to it is directly integrated on Si substrates. In addition, the BZTS thin film capacitors with the HfO_2 buffer layer also show very stable energy storage performance after He^+ and neutron irradiation with different doses, which provides experimental basis for the application of ultra-high energy storage thin film capacitors integrated with Si in harsh environments (such as high temperature, high cold, radiation environment, etc).

Author Contributions

Fan Zhao: Methodology, Investigation, Writing - original draft. **Yilin Wu:** Software. **Yanzhu Dai:** Investigation. **Guangliang Hu:** Validation. **Ming Liu:** Conceptualization, Methodology, Writing - review & editing, Supervision, Funding acquisition. **Runlong Gao:** Investigation. **Linyue Liu:** Writing - review & editing, Funding acquisition. **Xin Liu:** Investigation. **Yonghong Cheng:** Writing - review & editing. **Tianyi Hu:** Visualization. **Chunrui Ma:** Methodology, Writing - review & editing. **Dengwei Hu:** Writing - review & editing. **Xiaoping Ouyang:** Funding acquisition. **Chun-Lin Jia:** Writing - review & editing.

Conflicts of interest

There are no conflicts to declare.

Acknowledgements

This work was supported by National Natural Science Foundation of China (No. 51702255, No. 51390472 and No. 11922507), National Science Foundation of Shaanxi Province (No. 2019JM-068), National "973" projects of China (No. 2015CB654903), Fundamental Research Funds for the Central Universities, China Postdoctoral Science Foundation (No. 2015M582649), Open Fund of Key laboratory of Materials Preparation and Protection for Harsh Environment (Nanjing University of Aeronautics and Astronautics), Ministry of Industry and Information Technology (No. XCA19013-03).

Appendix A. Supporting information

Supplementary data associated with this article can be found in the online version.

References

1 B. J. Chu, X. Zhou, K. L. Ren, B. Neese, M. Lin, Q. Wang, F. Bauer and Q. M. Zhang, *Science*, 2006, **313,** 334-336.

2 L. T. Yang, X. Kong, F. Li, H. Hao, Z. X. Cheng, H. X. Liu, J. F. Li and S. J. Zhang, *Prog. Mater. Sci.*, 2019, **102,** 72-108.

3 Q. Li, K. Han, M. R. Gadinski, G. Z. Zhang and Q. Wang, *Adv. Mater*., 2014, **26,** 6244-6249.

4 Y. Tian, L. Jin, H. F. Zhang, Z. Xu, X. Y. Wei, E. D. Politova, S. Y. Stefanovich, N. V. Tarakina, I. Abrahams and H. X. Yan, *J. Mater. Chem. A*., 2016, **4,** 17279-17287.

5 H. Pan, A. Kursumovic, Y. H. Lin, C. W. Nan and J. L. MacManus-Driscoll, *Nanoscale*, 2020, **12,** 19582-19591.

6 B. C. Luo, X. H. Wang, E. Tian, H. Z. Song, H. X. Wang and L. T. Li, *ACS Appl. Mater. Interfaces*., 2017, **9,** 19963–19972.

7 Y. N. Hao, X. H. Wang, K. Bi, J. M. Zhang, Y. H. Huang, L. W. Wu, P. Y. Zhao, K. Xu, M. Lei and L. T. Li, *Nano Energy*, 2017, **31,** 49-56.

8 T. Wang, L. Jin, C. C. Li, Q. Y. Hu and X. Y. Wei, *J. Am. Ceram. Soc*., 2015, **98,** 559-566.

9 P. Liu, M. Y. Li, Q. F. Zhang, W. R. Li, Y. J. Zhang, M. Shen, S. Y. Qiu, G. Z. Zhang and S. L. Jiang, *J. Eur. Ceram. Soc*., 2018, **38,** 5396-5401.

10 J. Kim, S. Saremi, M. Acharya, G. Velarde, E. Parsonnet, P. Donahue, A. Qualls, D. Garcia and L. W. Martin, *Science*, 2020, **369,** 81-84.

11 M. D. Nguyen, C. T. Q. Nguyen, H. N. Vu and G. Rijnders, *Curr. Appl. Phys*., 2019, **19,** 1040-1045.

12 M. K. Bhattarai, K. K. Mishra, A. A. Instan, B. P. Bastakoti and R. S. Katiyar, *Appl. Surf. Sci*., 2019, **490,** 451-459.

13 Z. S. Liang, M. Liu, C. R. Ma, L. K. Shen, L. Lu and C. L. Jia, *J. Mater. Chem. A*., 2018, **6,** 12291-12297.

14 Z. S. Liang, C. R. Ma, L. K. Shen, L. Lu, X. L. Lu, X. J. Lou, M. Liu and C. L. Jia, *Nano Energy*, 2019, **57,** 519-527.

15 P. Yun, D. Y. Wang, Y. Wang and H. L. W. Chan, 2007 Sixteenth IEEE International Symposium on the Applications of Ferroelectrics, 2007, 519-527.

16 H. B. Cheng, J. Ouyang, Y. X. Zhang, D. Ascienzo, Y. Li, Y. Y. Zhao and Y. H. Ren, *Nat. Commun*., 2017, **8,** 1999.

17 A. A. Instan, S. P. Pavunny, M. K. Bhattarai and R. S. Katiyar, *Appl. Phys. Lett*., 2017, **111,** 142903.

18 M. D. Nguyen, C. T. Q. Nguyen, H. N. Vu and G. Rijnders, *J. Eur. Ceram. Soc*., 2018, **38,** 95-103.

19 T. Harter, S. Muehlbrandt, S. Ummethala, A. Schmid, S. Nellen, L. Hahn, W. Freude and C. Koos, *Nat. Photonics*., 2018, **12,** 625-633.

20 D. M. Sun, M. Y. Timmermans, Y. Tian, A. G. Nasibulin, E. I. Kauppinen, S. Kishimoto, T. Mizutani and Y. Ohno, *Nat. Nanotechnol*., 2011, **6,** 156-161.

21 S. H. Baek, J. Park, D. M. Kim, A. Aksyuk, R. R. Das, S. D. Bu, D. A. Felker, J. Lettieri, V. Vaithyanathan, S. S. N. Bharadwaja, N. Bassiri-Gharb, Y. B. Chen, H. P. Sun, C. M. Folkman, H. W. Jang, D. J. Kreft, S. K. Streiffer, R. Ramesh, X. Q. Pan, S. Trolier-McKinstry, D. G. Schlom, M. S. Rzchowski, R. H. Blick and C. B. Eom, *Science*, 2011, **334,** 958-961.

22 D. Birmpiliotis, P. Czarnecki, M. Koutsoureli, G. Papaioannou and I. D. Wolf, *Microelectron. Eng*., 2016, **159,** 209-214.

23 Q. L. Fan, C. R. Ma, Y. Li, Z. S. Liang, S. Cheng, M. Y. Guo, Y. Z. Dai, C. S. Ma, L. Lu, W. Wang, L. H. Wang, X. J. Lou, M. Liu, H. Wang and C. L. Jia, *Nano Energy*, 2019, **62,** 725-733.

24 K. T. Kim, G. H. Kim, J. C. Woo and C. Ⅱ. Kim, *J. Vac. Sci. Technol. A*., 2008, **26,** 1178-1181.
25 Q. L. Fan, M. Liu, C. R. Ma, L. X. Wang, S. P. Ren, L. Lu, X. J. Lou and C. L. Jia, *Nano Energy*, 2018, **51,** 539-545.
26 Q. L. Fan, C. S. Ma, C. R. Ma, R. Lu, S. Cheng and M. Liu, *Appl. Phys. Lett*., 2020, **116,** 192902.
27 J. P. B. Silva, J. M. B. Silva, M. J. S. Oliveira，T. Weingärtner, K. C. Sekhar, M. Pereira and M. J. M. Gomes, *Adv. Funct. Mater*., 2019, **29,** 1807196.
28 J. P. B. Silva, J. M. B. Silva, K. C. Sekhar, H. Palneedi, M. C. Istrate, R. F. Negrea, C. Ghica, A. Chahboun, M. Pereira and M. J. M. Gomes, *J. Mater. Chem. A*., 2020, **8,** 14171-14177.
29 C. H. Chien, D. Y. Wang, M. J. Yang, P. Lehnen, C. C. Leu, S. H. Chuang, T. Y. Huang and C. Y. Chang, *IEEE Electron Device Lett*., 2003, **24,** 553-555.
30 M. H. Park, H. J. Kim, Y. J. Kim, T. Moon, K. D. Kim and C. S. Hwang, *Adv. Energy. Mater*., 2014, **4,** 1400610.
31 X. L. Wang, L. Zhang, X. H. Hao and S. L. An, *Mater. Res. Bull*., 2015, **65,** 73-79.
32 J. Ge, D. Remiens, J. Costecalde, Y. Chen, X. L. Dong and G. S. Wang, *Appl. Phys. Lett*., 2013, **103,** 162903.
33 C. W. Ahn, G. Amarsanaa, S. S. Won, S. A. Chae, D. S. Lee and I. W. Kim, *ACS Appl. Mater. Interfaces*., 2015, **7,** 26381-26386.
34 X. L. Wang, L. W. Zhang, X. H. Hao, S. L. An and B. Song, *J. Mater. Sci: Mater. Electron*., 2015, **26,** 9583-9590.
35 L. Zhang, M. Liu, W. Ren, Z. Y. Zhou, G. H. Dong, Y. J. Zhang, B. Peng, X. H. Hao, C. Y. Wang, Z. D. Jiang, W. X. Jing and Z. G. Ye, *RSC. Adv*., 2017, **7,** 8388-8393.
36 Y. Yao, Y. Li, N. N. Sun, J. H. Du, X. W. Li, L. W. Zhang, Q. W. Zhang and X. H. Hao, *J. Alloys. Compd*., 2018, **750,** 228-234.
37 M. D. Nguyen, E. P. Houwman, M. T. Do and G. Rijnders, *Energy. Storage. Mater*., 2020, **25,** 193-201.
38 M. D. Nguyen and G. Rijnders, *J. Eur. Ceram. Soc*., 2018, **38,** 4953-4961.

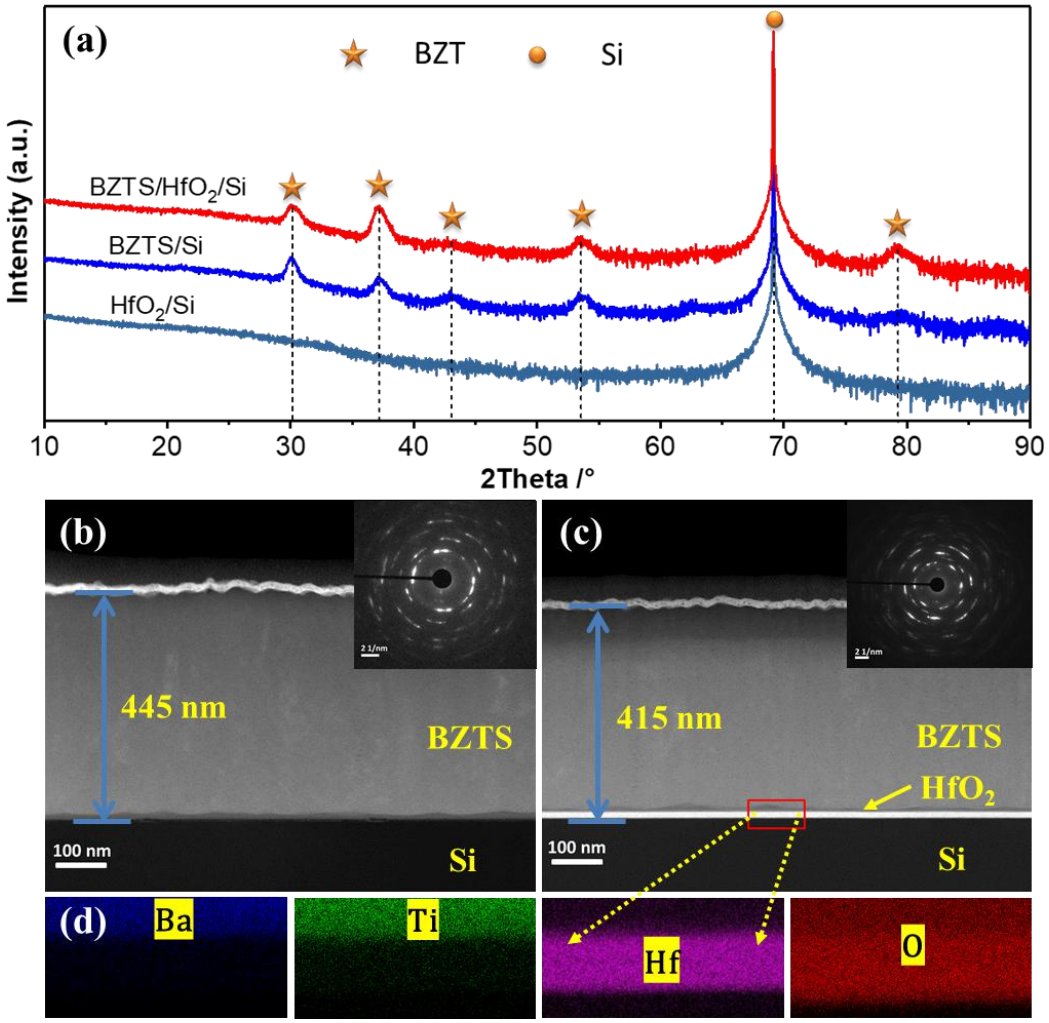

Fig. 1 (a) Typical XRD θ–2θ scans of the HfO_2, BZTS and BZTS/HfO_2 thin films on Si substrates. (b), (c) Low magnification dark field STEM images of the BZTS/Si (b) and the BZTS/HfO_2/Si (c) heterostructure. Insets of (b) and (c) are corresponding selected area electron diffraction (SAED) patterns on BZTS with 0.1 nm beam size for the BZTS and the BZTS/HfO_2 films. (d) Element mapping of the sample area covered by the red box in Fig 1(c).

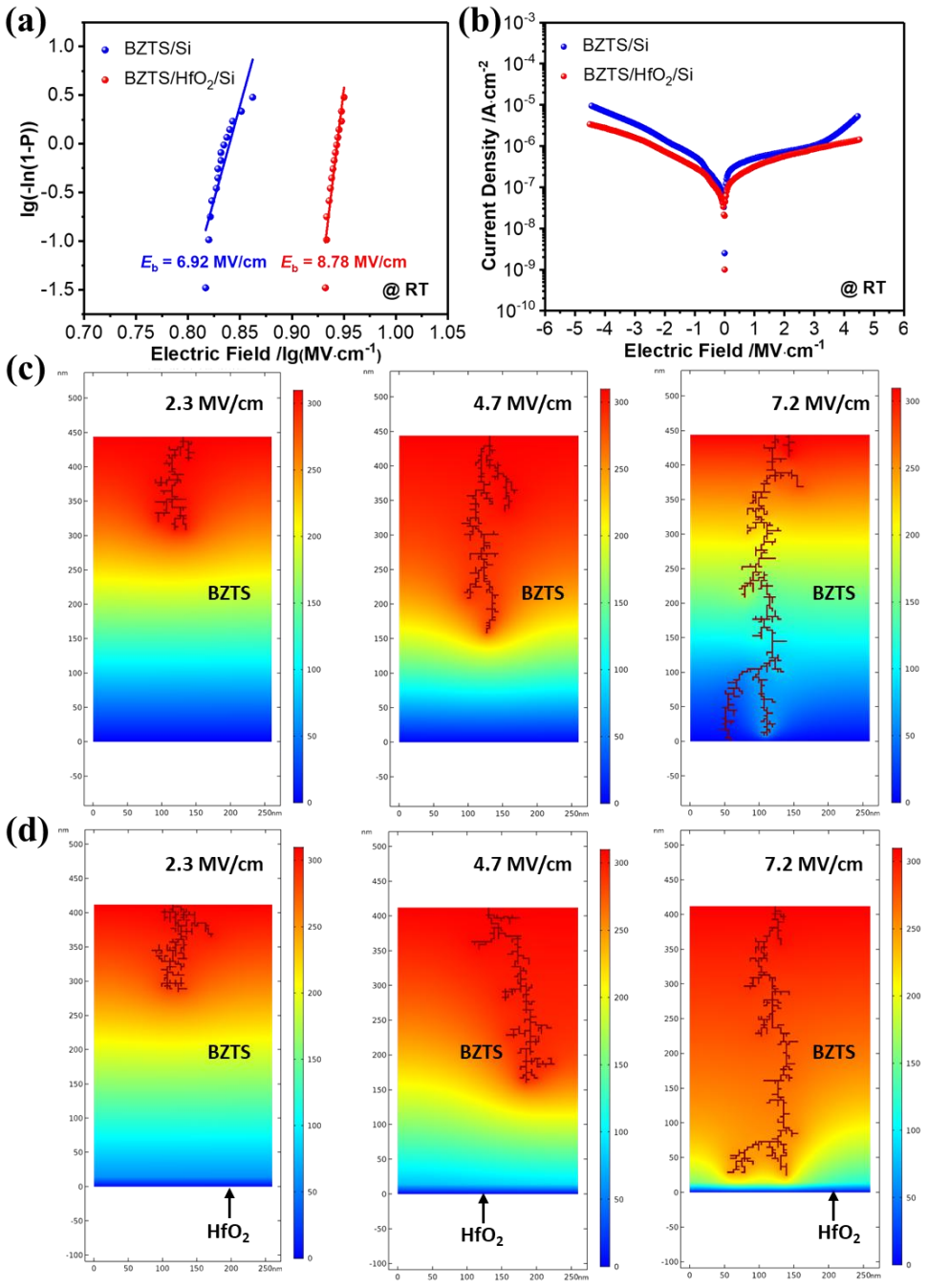

Fig. 2 (a) The Wei-bull distribution of E_b for the BZTS thin films and the BZTS/HfO_2 thin films. (b) The leakage current density of the BZTS and the BZTS/HfO_2 films as a function of the electric field. (c), (d) The electric tree simulation results for (c) BZTS and (d) BZTS/HfO_2 thin films under various applied electric field (2.3 MV/cm, 4.7 MV/cm, 7.2 MV/cm).

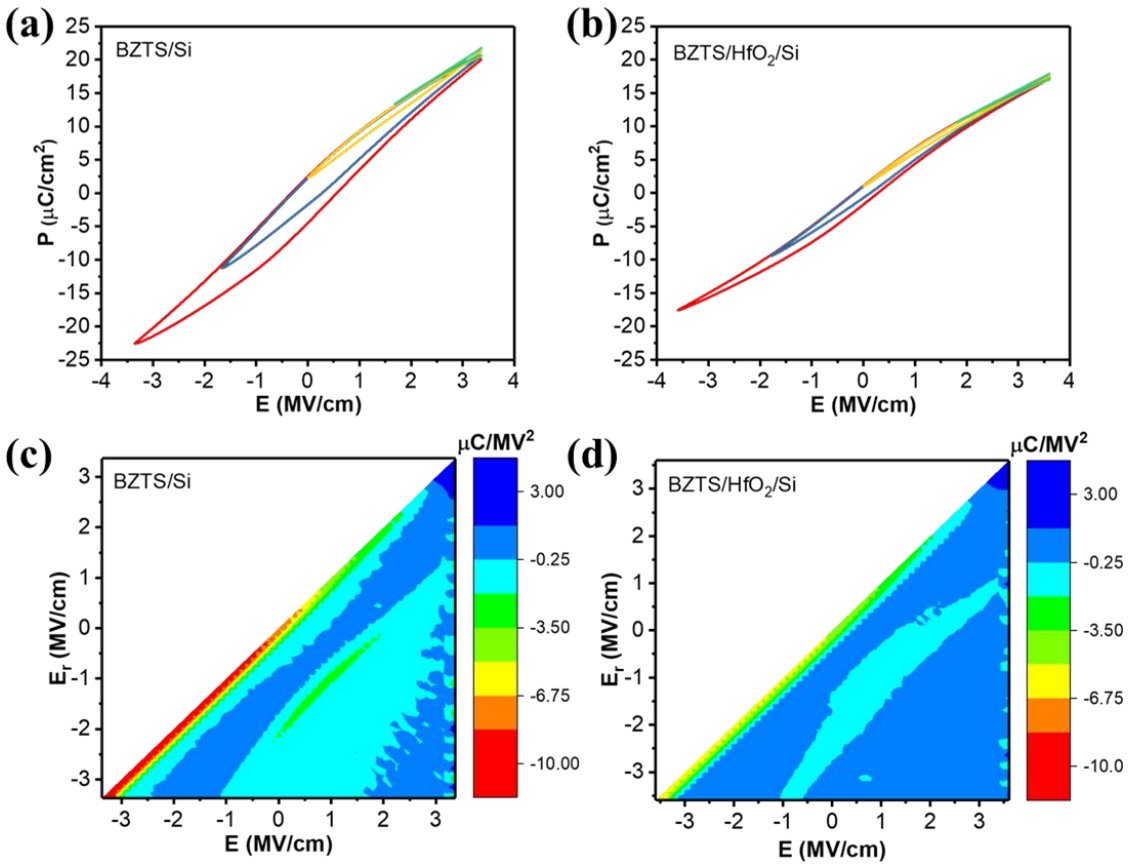

Fig. 3 (a), (b) FORC loops of the BZTS thin film capacitors and the BZTS/HfO_2 thin film capacitors, respectively (only four of the total 60 loops are shown for clarity). (c), (d) Corresponding FORC distribution ρ (E_r, E) of the BZTS thin film capacitors and the BZTS/HfO_2 thin film capacitors.

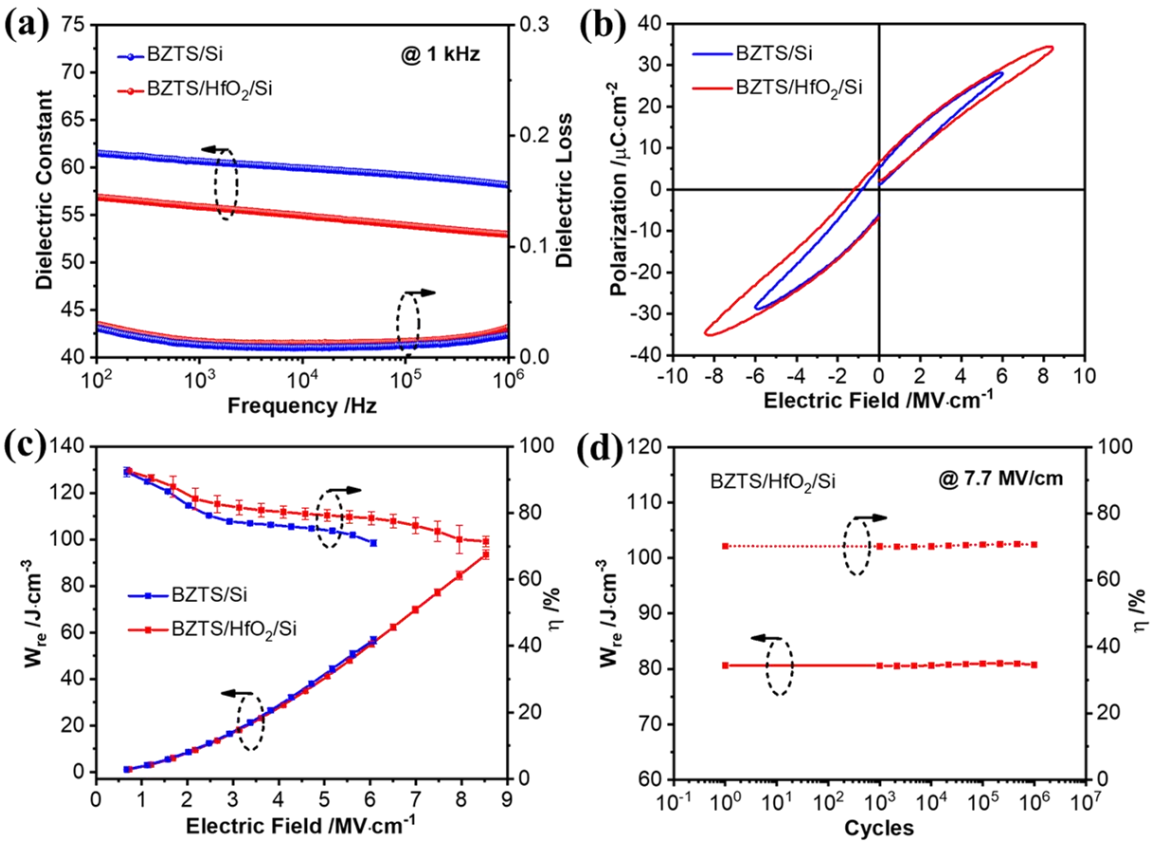

Fig. 4 (a) Frequency dependence of dielectric constant (ε_r) and dielectric loss (tanδ) at RT for the BZTS thin films and the BZTS/HfO_2 thin films. (b) *P-E* hysteresis loops of the BZTS thin films and the BZTS/HfO_2 thin films. (c) The W_{re} and η of the BZTS thin films and the BZTS/HfO_2 thin films depending on electric field. (d) The W_{re} and η of the BZTS/HfO_2 thin films during 10^6 charge-discharge cycles.

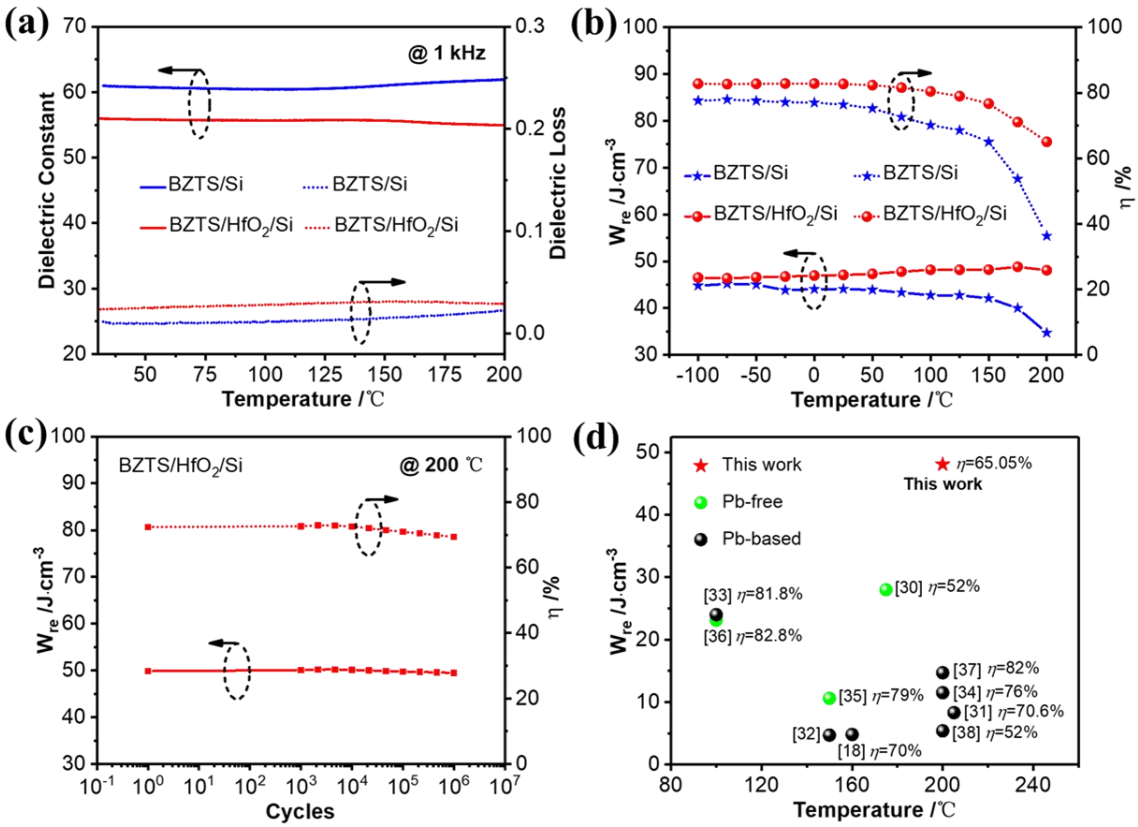

Fig. 5 (a) Temperature dependence of ε_r and tanδ at 1 kHz for the BZTS thin film capacitors and the BZTS/HfO_2 thin film capacitors. (b) The W_{re} and η as a function of temperature for the BZTS thin film capacitors and the BZTS/HfO_2 thin film capacitors under the electric field of 5.35 MV/cm. (c) The W_{re} and η of the BZTS/HfO_2 thin film capacitors during the 10^6 charge-discharge cycles at 200 °C. (d) Comparison with some of the recently reported wide temperature energy storage performances of thin film capacitors grown on Si substrates by physical method.

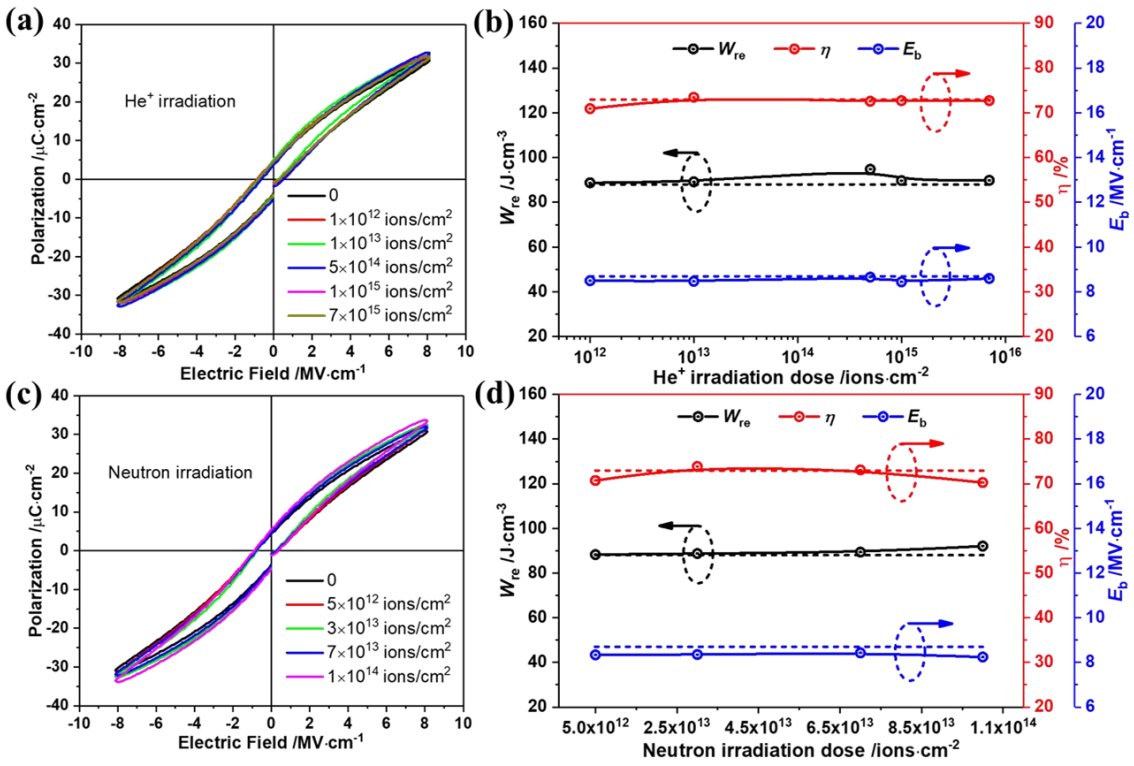

Fig. 6 (a) The room temperature *P-E* hysteresis loops of the BZTS/HfO_2 thin film capacitors irradiated by 3MeV He^+ ions with different doses, and the applied electric field was 8.2 MV/cm. (b) The W_{re}, η and E_b calculated from the *P-E* hysteresis loops in figure (a) as a function of the irradiation dose. The dotted line in the figure represents the energy storage performance of the un-irradiated sample. (c) The room temperature *P-E* hysteresis loops of the BZTS/HfO_2 thin film capacitors irradiated by neutron with an average energy of 1 MeV and irradiation dose ranging from 5×10^{12} ions/cm^2 to 1×10^{14} ions/cm^2, and the applied electric field was 8.2 MV/cm. (d) The W_{re}, η and E_b calculated from the *P-E* hysteresis loops in figure (c) as a function of the irradiation dose.